Supporting Information for:

Electron-losing regulation strategy for stripping modulation towards highly reversible Zn Anode

Xinyi Wang‡[a,b], Liyang Liu‡[a], Zewei Hu[a], Chao Han[c], Xun Xu[b], Shixue Dou[b,d], Weijie Li*[a,b]

[a]State Key Laboratory for Powder Metallurgy, Central South University, Changsha 410083, China.

[b]Institute for Superconducting and Electronic Materials, Australian Institute for Innovative Materials, University of Wollongong, Wollongong, NSW 2522, Australia.

[c]School of Materials Science and Engineering, Central South University, Changsha 410083, China.

[d]Institute of Energy Materials Science, University of Shanghai for Science and Technology, Shanghai, 200093, China

E-mail: li-306@csu.edu.cn

1. Experimental Procedures

1.1 Electrolyte Preparation.

The $Zn(OTF)_2$ electrolytes were prepared by directly adding Zn $(CF_3SO_3)_2$ into H_2O to form a 2 mol kg^{-1} (*m*) electrolyte. The volume ratios of oxolane (OL)/H_2O were controlled 0, 5, 7.5, 10, 20, 30 and 40 vol % and denoted as OL 0, OL 5, OL 7.5, OL 10, OL 20, OL 30 and OL 40, respectively.

1.2 Preparation of NVO cathode materials.

The $NaV_3O_8 \cdot 1.5H_2O$ (NVO) nanobelts were prepared based on the previous report.[1] Typically, commercial V_2O_5 powder (1 g) and 2M NaCl aqueous solution (15 mL) were mixed. Then, the mixture was stirred for 96 h at 30 °C. During the stirring, the color of the mixture changed from orange to dark red. After being filtered and washed with deionized water and ethanol three times, the resultant powder (NVO) was obtained by drying at 80 °C for 12 h.

1.3 Materials.

Zinc trifluoromethanesulfonate (Zn $(CF_3SO_3)_2$, ≥99%), oxolane (99%), sodium chloride (NaCl, ≥99.5%) and V_2O_5 (≥98%) were purchased from Sigma-Aldrich.

1.4 Materials Characterizations.

The XRD measurements were performed on PANalytical Aeris X-ray diffractometer with Cu Kαradiation (λ= 1.5406 Å) at a scanning rate of 2° min^{-1}. The morphology and structure of samples were checked by the field-emission scanning electron microscope (JEOL JSM-7500FA) and a scanning laser confocal microscopy (SLCM, KEYENCE VK-X150). XPS measurements were carried out on a Thermo Fisher Scientific ESCALAB (Al Kα radiation, hv =1486.6 eV). Ar^+ sputtering with a power of 3,000 eV was used to investigate the composition of the passivation layer. The binding energies were referenced to the C 1s peak at 284.8 eV. FTIR results were obtained on the PerkinElmer Frontiers instrument. Raman spectra were collected from a Raman spectrometer (Thermo Fischer DXR) by using an excitation wavelength of 532 nm. The ^1H NMR spectra of the electrolytes were performed on Bruker Avance III 600 MHz equipment.[2] The ionic conductivity of different electrolytes was performed on a Mettler Toledo FE38 conductivity meter. The contact angle tests were conducted on the Data Physics OCA 25 instrument. The in situ optical micrographs during Zn stripping were obtained from the Leica M205A stereo Microscope. *In-situ* XRD was conducted

at the Powder Diffraction beamline, Australian Synchrotron (ANSTO). The wavelength was 0.6885 Å using the NIST LaB6 660b standard reference material.

1.5 Electrochemical measurements

All cells were assembled using coin-type cells (CR 2032) in air at room temperature with the use of Zn foil (100 μm) as the anode, glass fiber (GF/D) as the separator, as-prepared electrolytes (80 μL) as the electrolyte. Two pieces of symmetric Zn foils (φ = 14 mm) were employed as electrodes for Zn|Zn symmetric cells. The Zn|Cu cells were assembled with Zn foil (φ = 14 mm) as anode and Cu (φ = 14 mm) as cathode with cut-off voltage of 0.5V. The NVO electrodes were prepared by blending as-synthesized NVO powder, Super P, and polyvinylidene difluoride (PVDF) in a weight ratio of 7:2:1 in the presence of 1-methyl-2-pyrrolidone (NMP). After coating the resultant slurry on stainless steel (SS) meshes, the SS meshes were dried in a vacuum oven at 80 °C for 12 h. The mass loading of active materials was controlled as ∼1.5 mg cm^{-2}. All assembled cells were allowed to stand for 5 h before testing. The electrochemical measurements were performed on a NEWARE coin cell tester and a Biologic VMP-3 electrochemical workstation. CA curves were obtained at a fixed overpotential of -150 mV in Zn symmetric cells. The LSV curves were obtained by scanning the voltage at a rate of 0.5 mV s^{-1}, ranging from 0.2 to −0.5 V. The frequency range of EIS is from 1 MHz to 10 mHz. CV profiles of Zn|NVO cells were measured at a scan rate of 0.1 mV s^{-1} between 0.3 and 1.4 V.

1.6 Computation methods

All the calculations are performed in the framework of the density functional theory within the Cambridge Sequential Total Energy Package (CASTEP).[3] The generalzied gradient approximation proposed by Perdew-Burke-Ernzerhof (PBE) is selected for the exchange-correlation potential.[4] The cut-off energy for the plane wave is set to 450 eV. The energy criterion is set to 10^{-5} eV in the iterative solution of the Kohn-Sham equation. All the structures are relaxed until the residual forces on the atoms have declined to less than 0.02 eV/Å. To avoid interlaminar interactions, a vacuum spacing of 15 Å is applied perpendicular to the slab.

The FORCITE module with COMPASS III force field in Material Studio 2023 was utilized to conduct Molecular Dynamics (MD) simulations. Initially, full optimization of each solution component-H_2O, OL, and $CF_3SO_3^-$-was performed. Subsequently, three distinct solutions named OL 0, OL 7.5, and OL 40 were assembled within a single cubic cell with dimensional length of 41.55 Å. Table S2 shows the respective quantities of solution components in these

systems. Following the structure optimization, equilibrium simulations were executed for 2000 ps in the NPT ensemble under constant pressure (1.0 atmosphere) and temperature (298 K). The time step used was 1fs. The simulations were conducted within a cubic box employing periodic boundary conditions in all directions. Upon achieving an equilibrium state, MD simulations were rerun in the NVT ensemble (T = 298 K) for 10000 ps, employing the Nose-Hoover thermostat. Throughout this process, simulation trajectories were recorded at intervals of every 25000 steps.

2. Supplementary figures

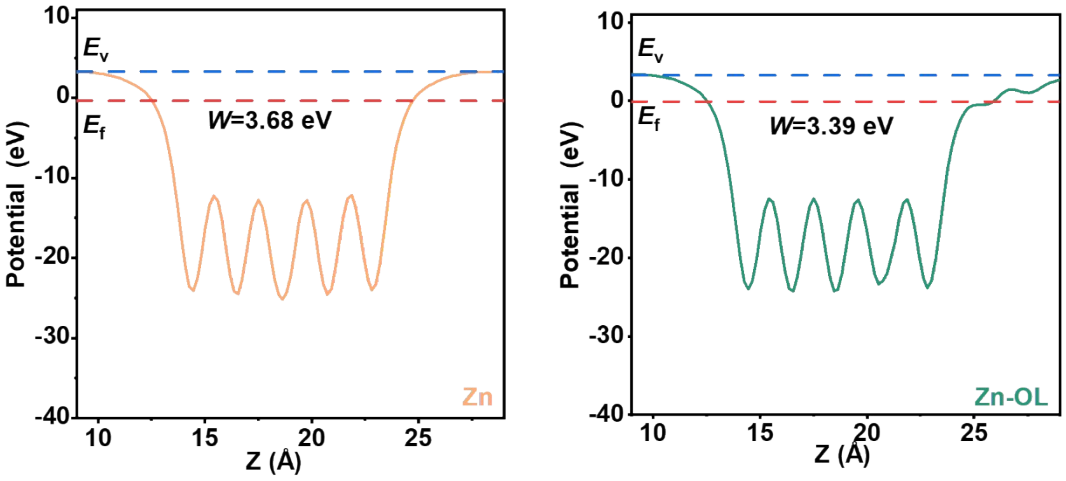

Figure S1. The work function of Zn (101) with and without OL.

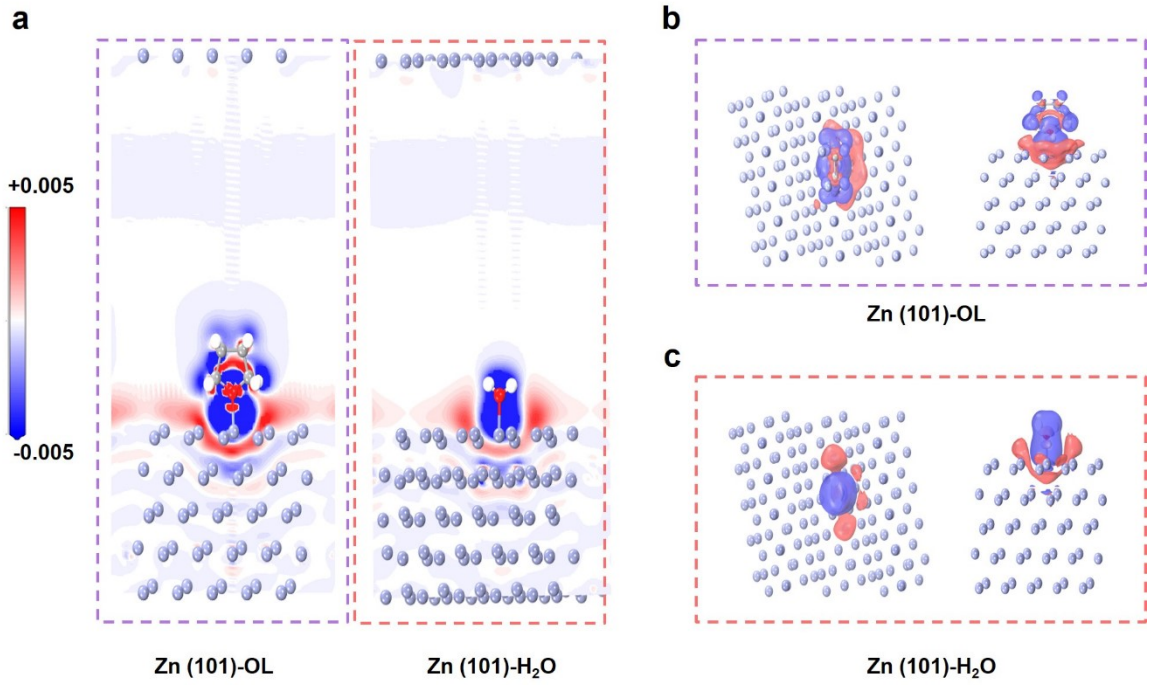

Figure S2. (a) Charge density difference of OL and H_2O on Zn (101). Red colour means electrons accumulating, bule means electrons losing. (b) and (c) Top view, side view 3D image of charge density difference of OL and H_2O on Zn (101).

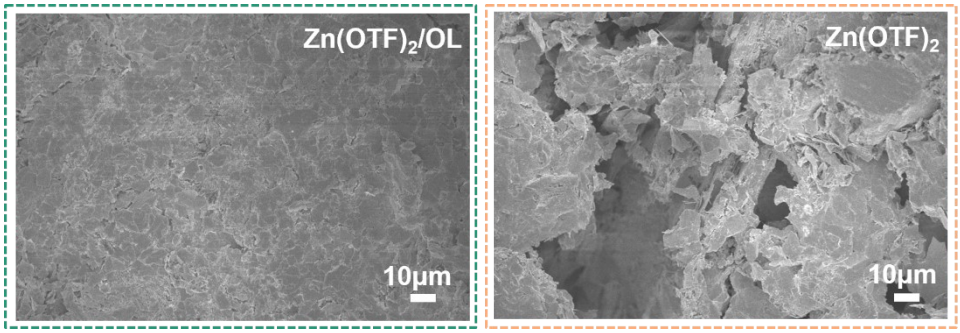

Figure S3. SEM images of anodes after stripping 10h in different electrolytes.

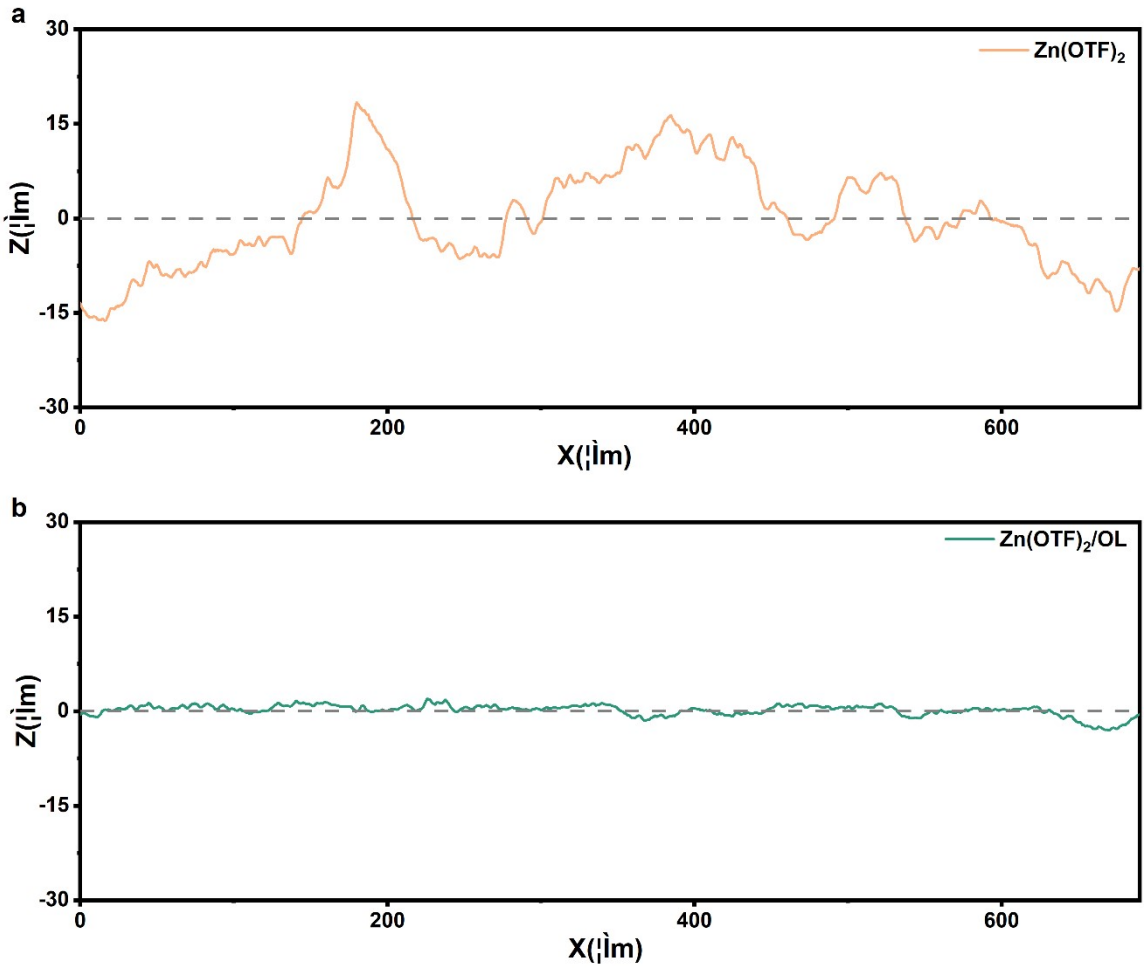

Figure S4. The line roughness of the Zn electrode with and without OL.

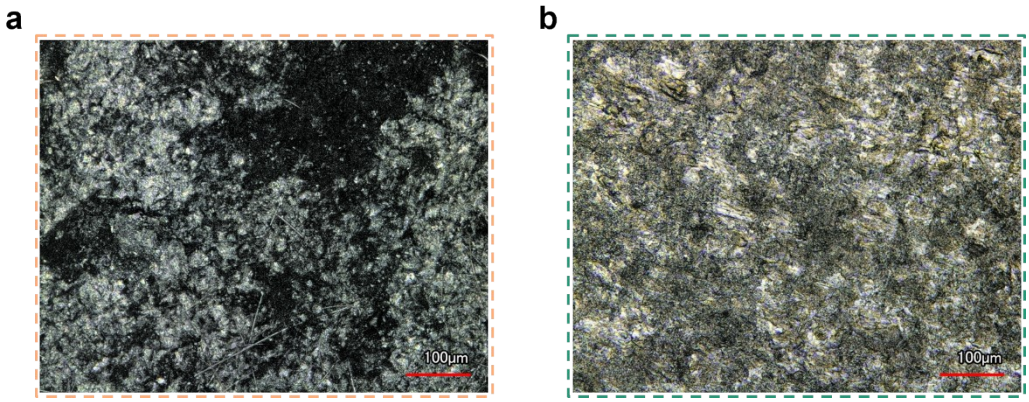

Figure S5 Digital images of Zn electrodes in (a) $Zn(OTF)_2$ and (b) $Zn(OTF)_2$/OL.

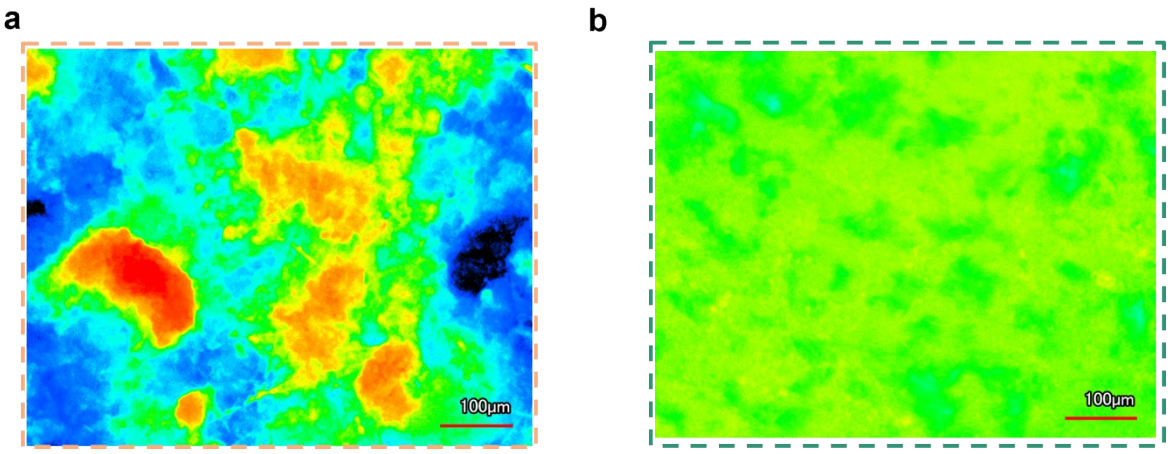

Figure S6. Top view of 2D version of Zn electrodes in (a) $Zn(OTF)_2$ and (b) $Zn(OTF)_2$/OL.

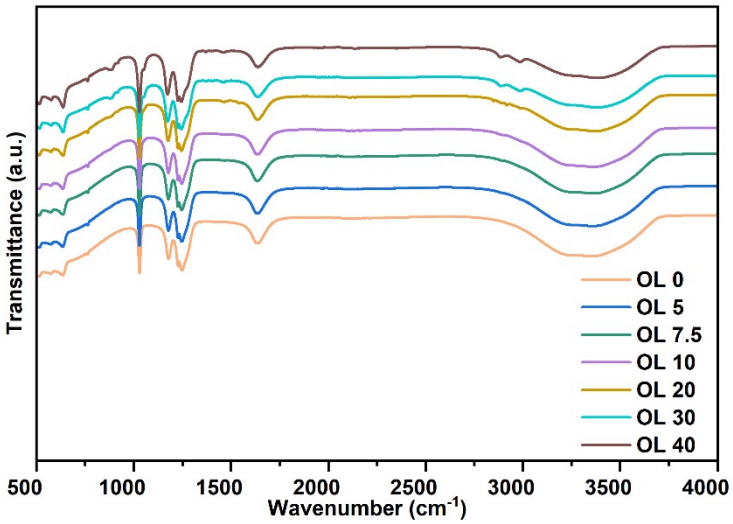

Figure S7. FTIR spectra of the OL 0, OL 5, OL 7.5, OL 10, OL 20, OL 30 and OL 40 electrolytes.

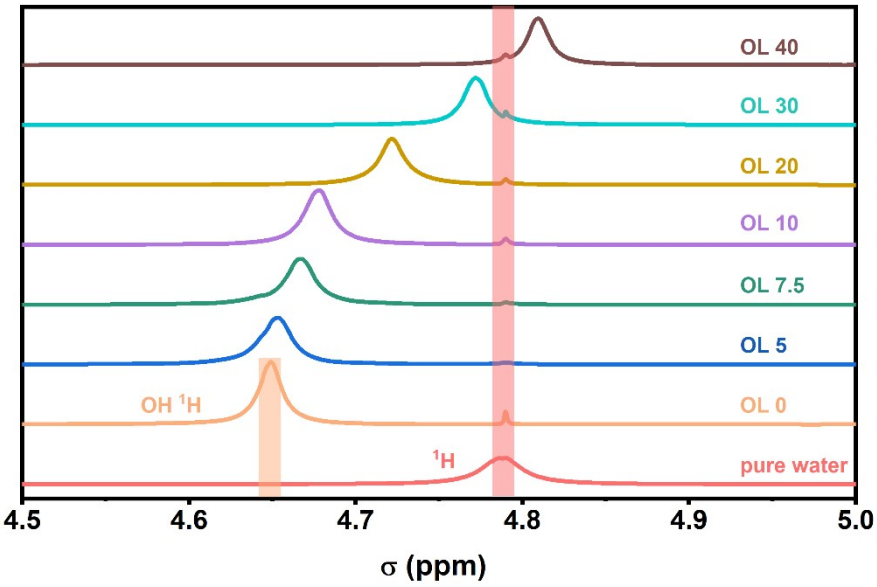

Figure S8. ^{1}H NMR spectra of the OL 0, OL 5, OL 7.5, OL 10, OL 20, OL 30 and OL 40 electrolytes.

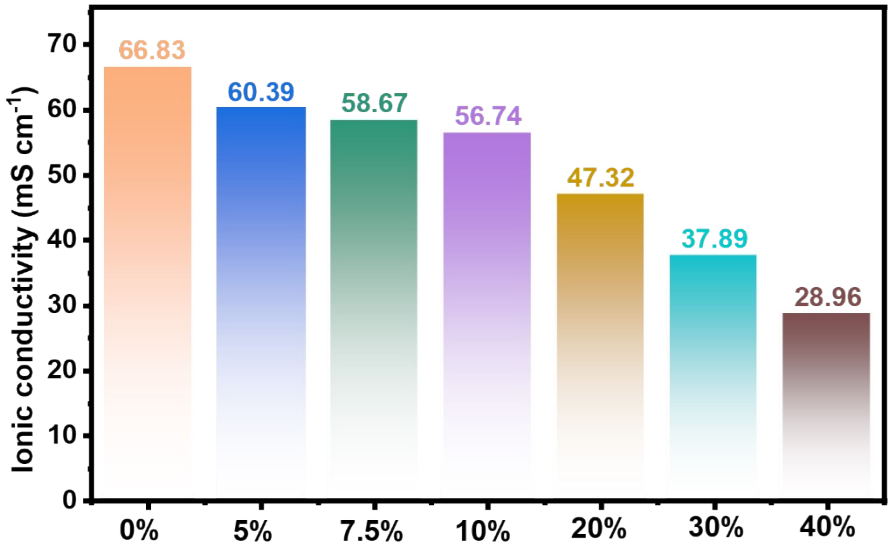

Figure S9. Measured ionic conductivity of the OL 0, OL 5, OL 7.5, OL 10, OL 20, OL 30 and OL 40 electrolytes.

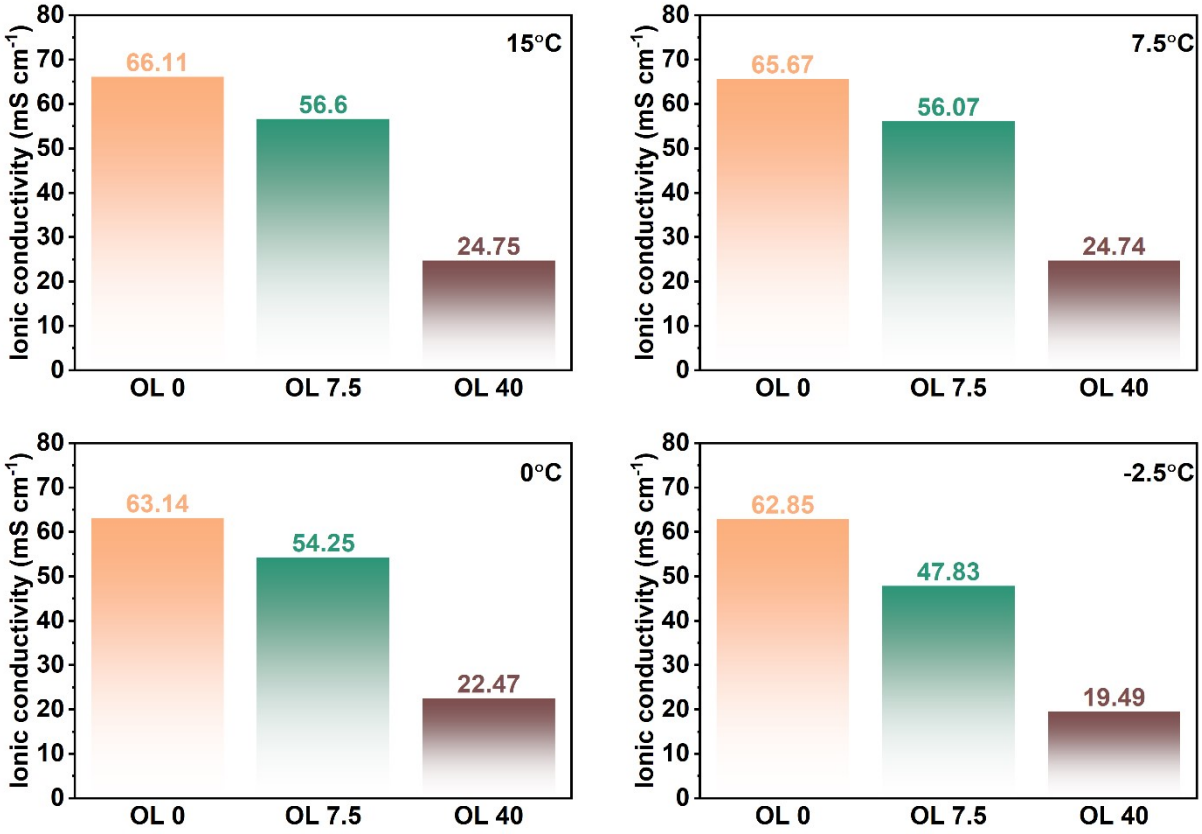

Figure S10. Measured ionic conductivity of the OL 0, OL 7.5 and OL 40 electrolytes at different temperatures.

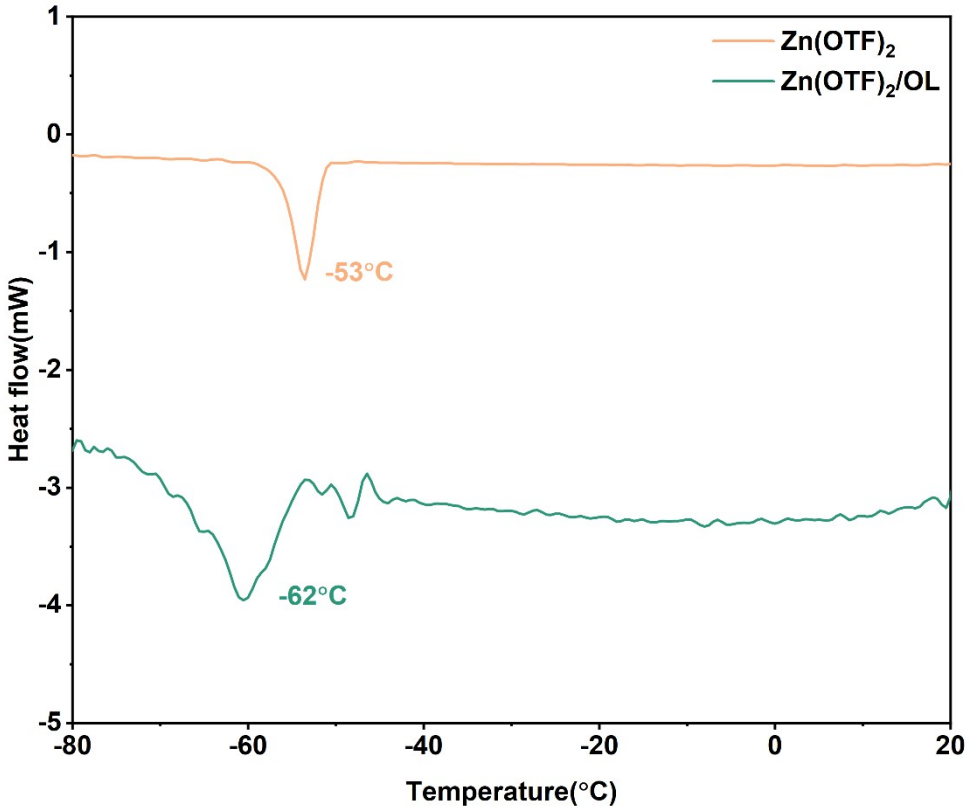

Figure S11. The Differential scanning calorimetry (DSC) curves of different electrolytes.

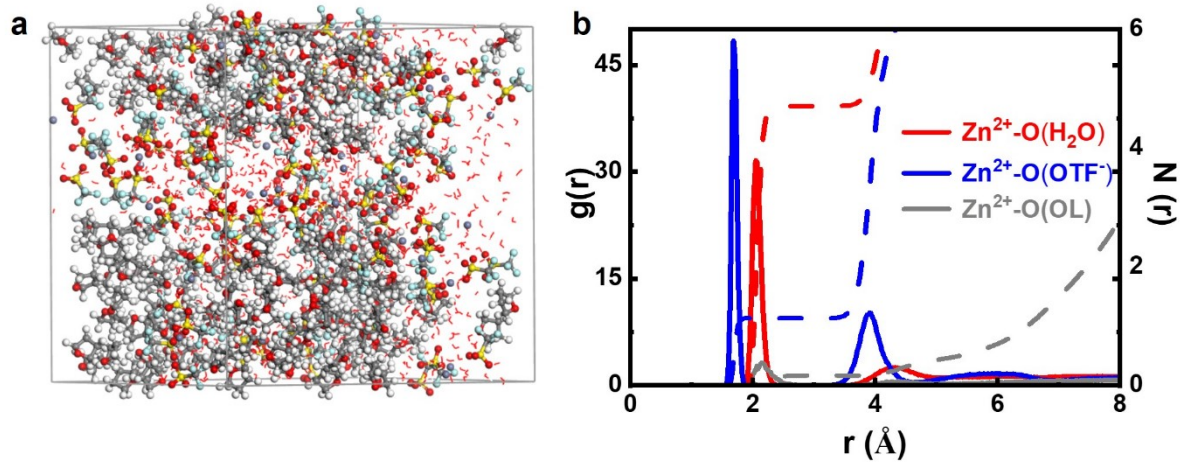

Figure S12. (a) MD simulation snapshots for OL 40. (b) RDF plots for OL 40.

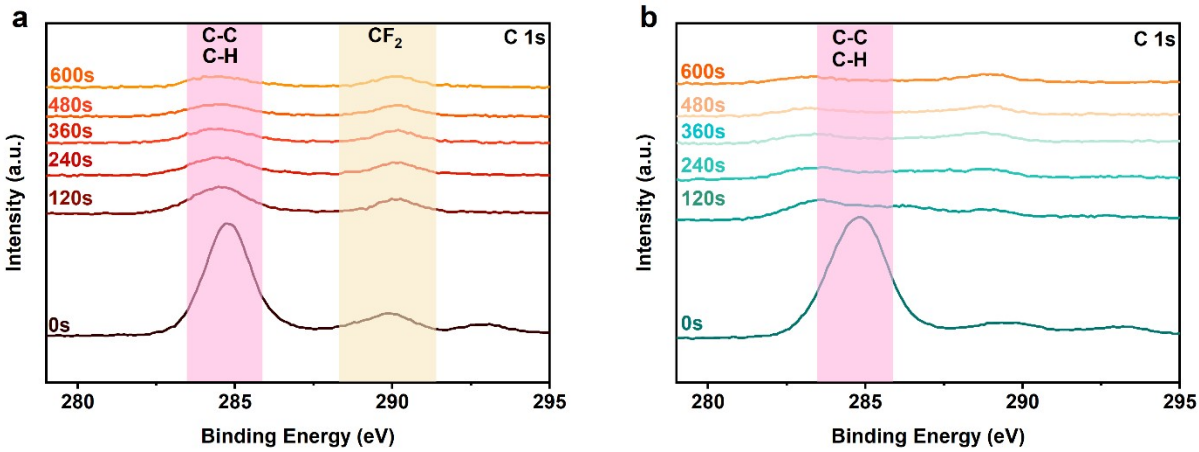

Figure S13. The XPS results of electrode in (a) $Zn(OTF)_2$ and (b) $Zn(OTF)_2$/OL.

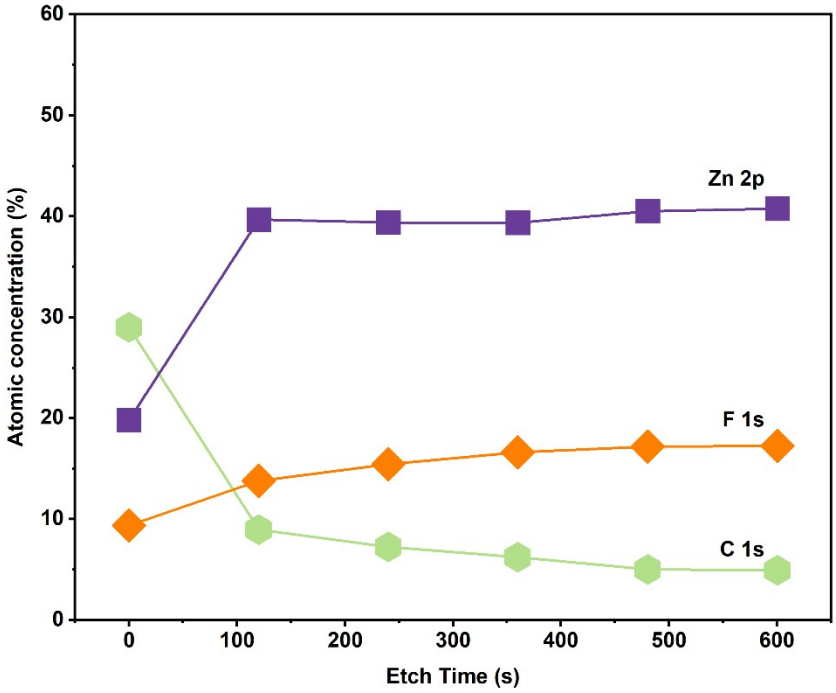

Figure S14. atomic concentrations of electrode in $Zn(OTF)_2$/OL.

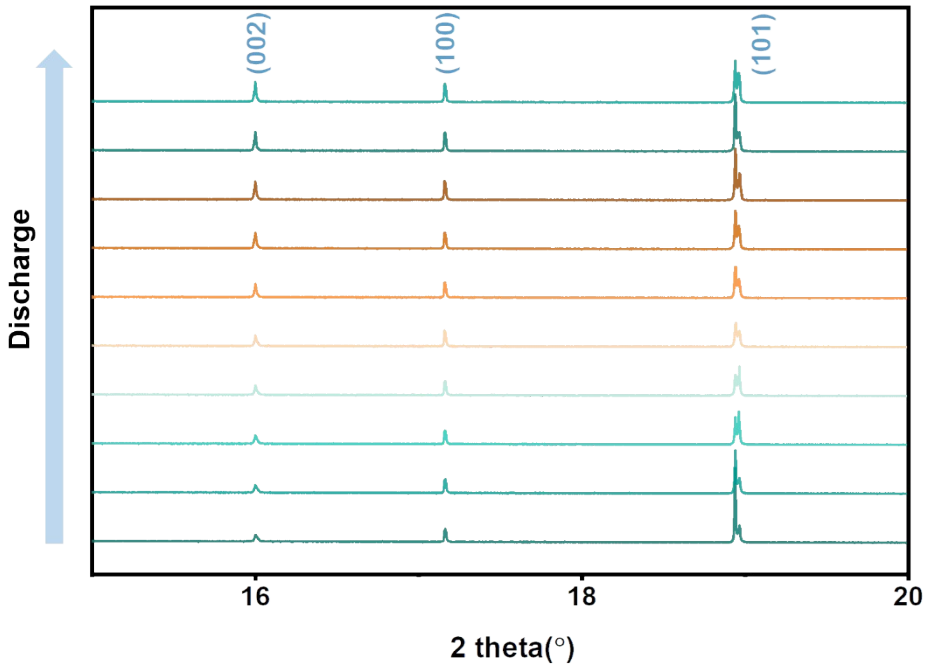

Figure S15. *In-situ* XRD Patterns of deposited Zn plates.

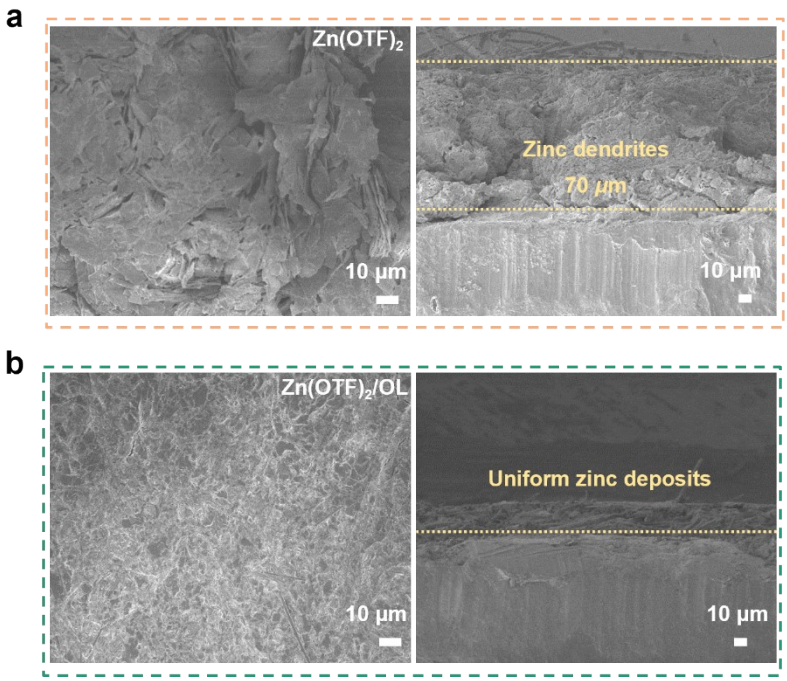

Figure S16. Zn electrodes in symmetrical cells after 50 cycles at 2 mA cm^{-2} and 2 mA h cm^{-2}.

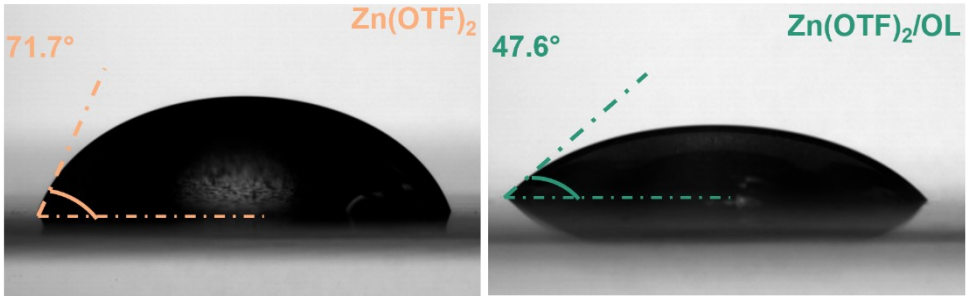

Figure S17. Contact angle measurements of bare Zn in different electrolytes.

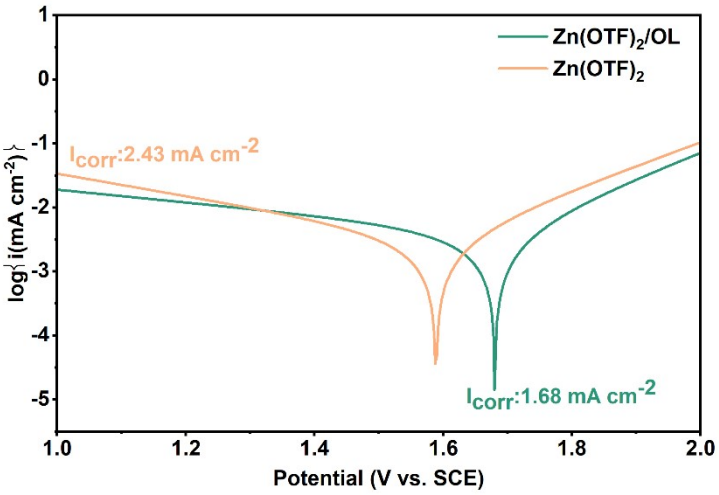

Figure S18. Tafel plots of Zn anodes in different electrolytes.

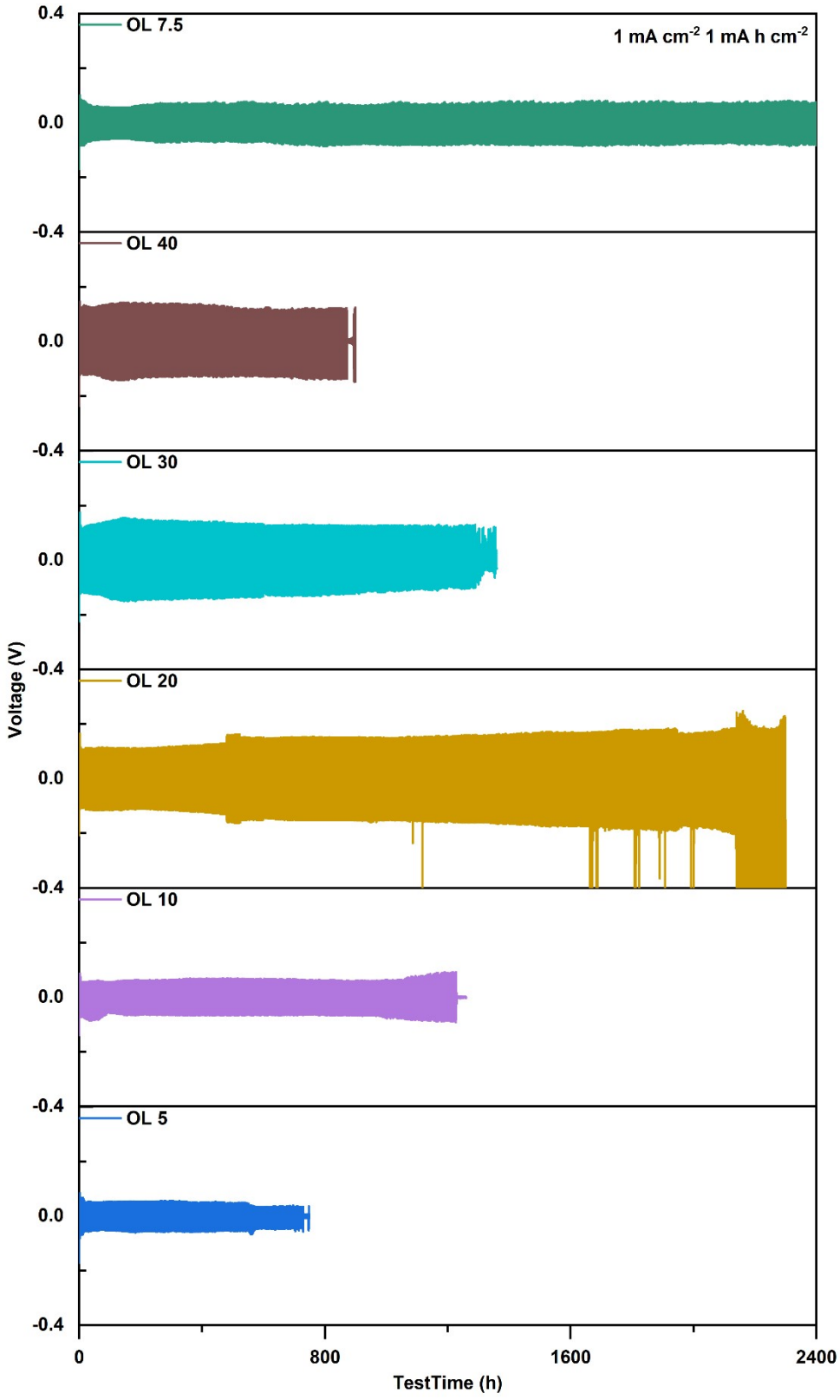

Figure S19. Cycle performance for Zn||Zn symmetric cells using 2m $Zn(OTF_2)$electrolyte with different volume percent of OL at 1 mA cm^{-2} and 1 mA h cm^{-2}.

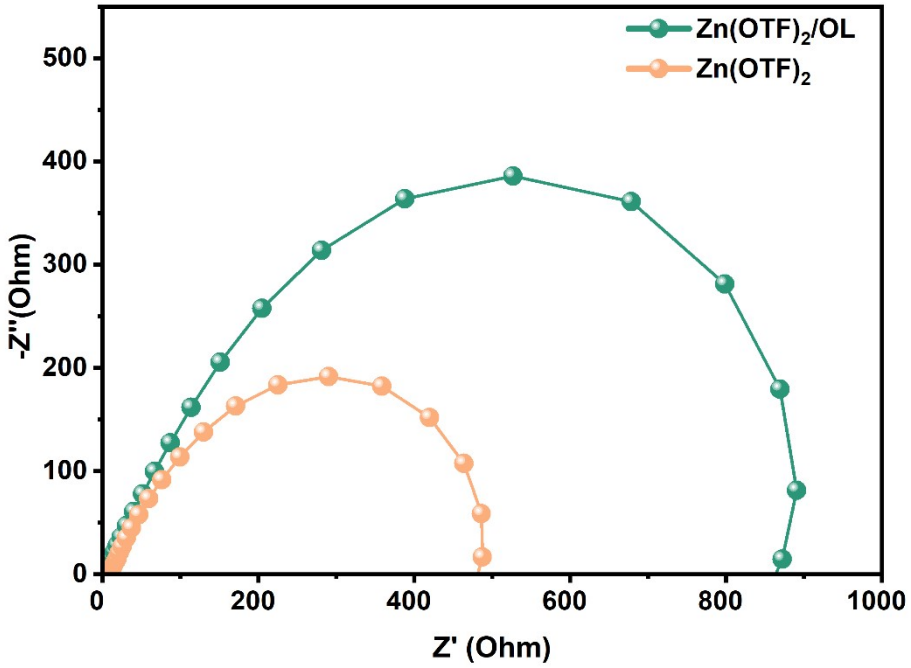

Figure S20. Nyquist plots of Zn||Zn symmetric cells with/without additive.

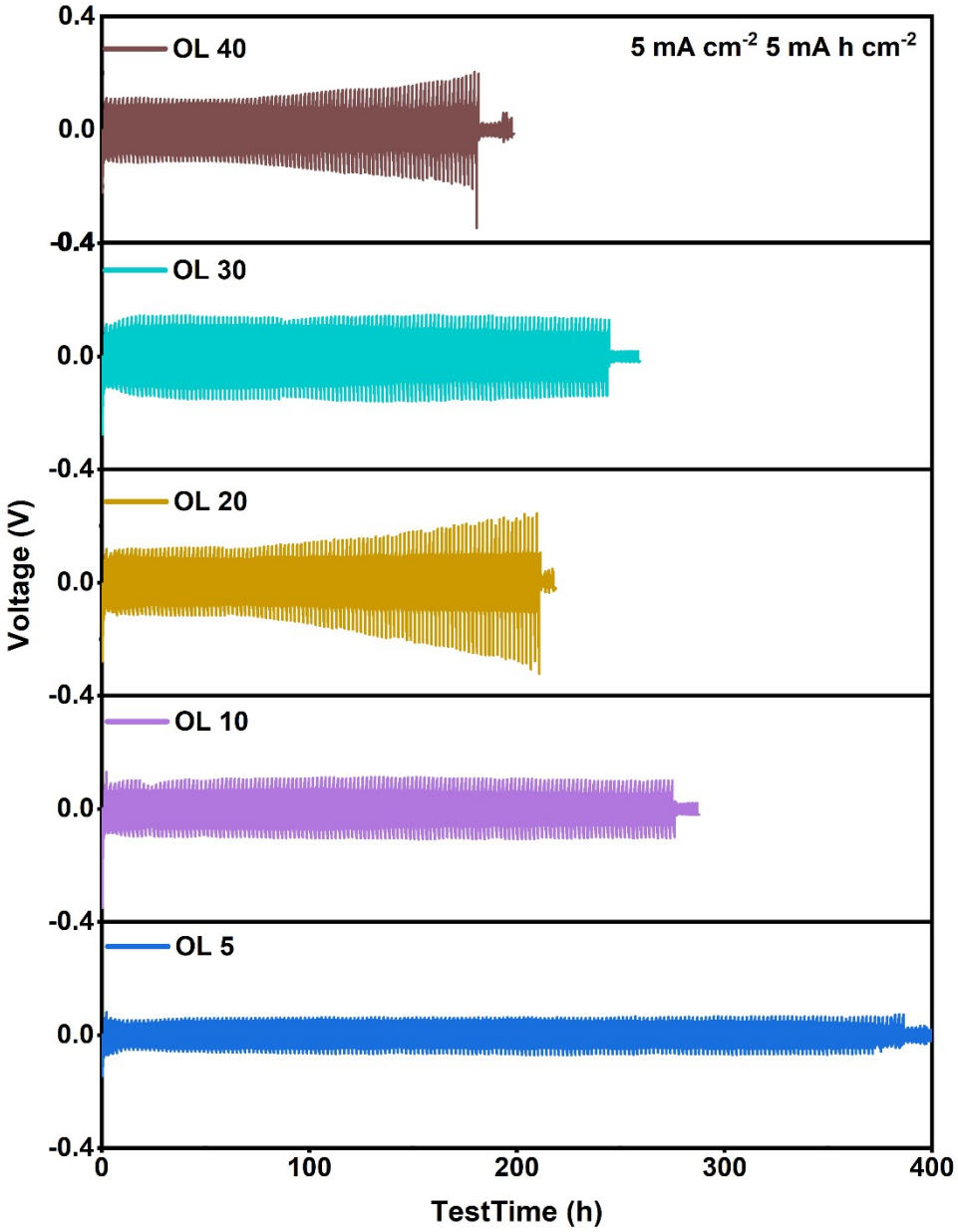

Figure S21. Cycle performance for Zn||Zn symmetric cells using 2m $Zn(OTf)_2$ electrolyte with different volume percent of OL at 5 mA cm^{-2} and 5 mA h cm^{-2}.

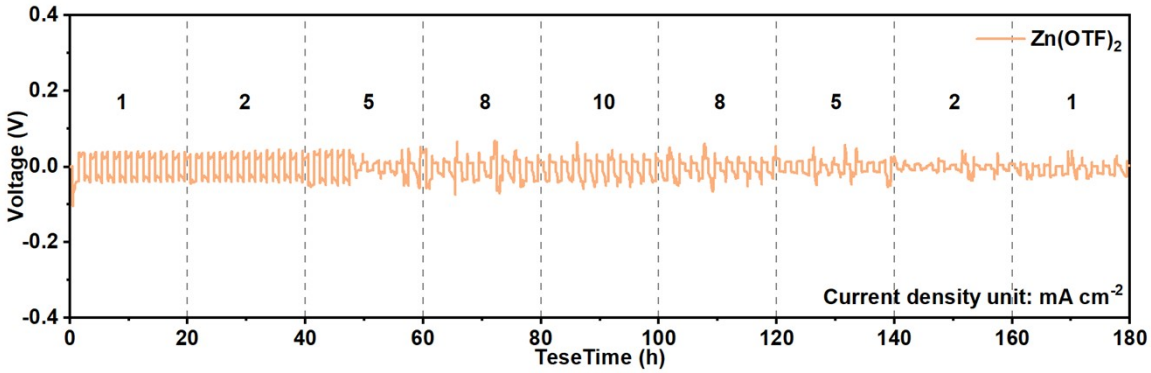

Figure S22. The rate performance of Zn symmetric cell using $Zn(OTF)_2$ electrolyte.

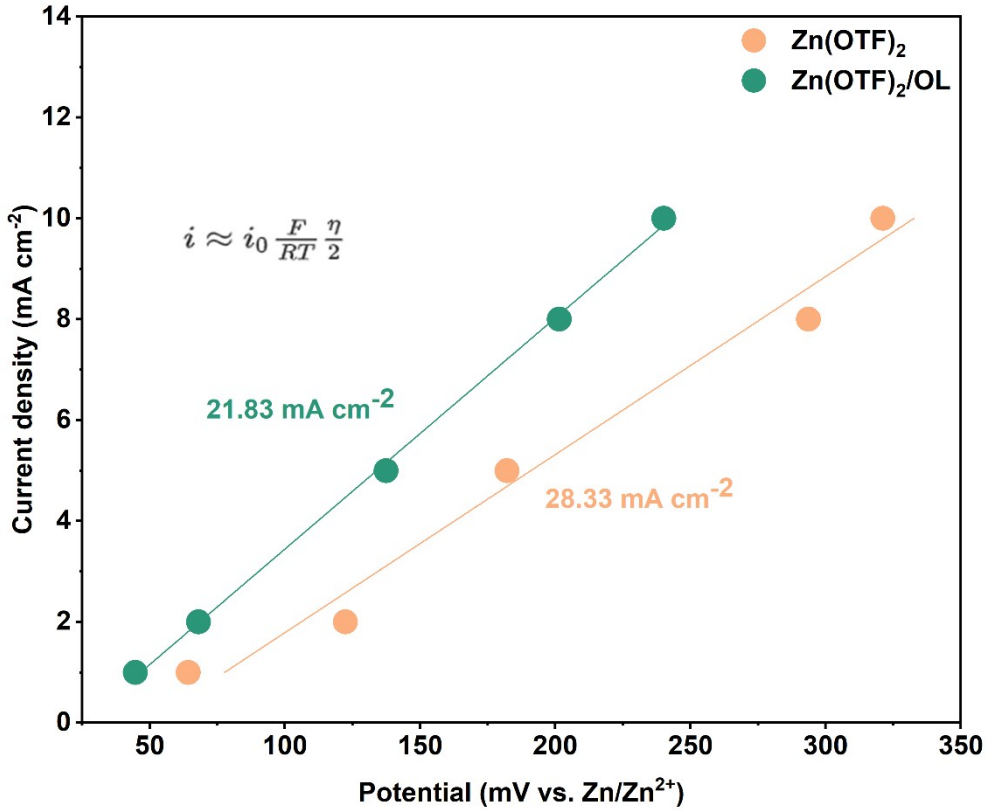

Figure S23. Calculated exchange density of Zn asymmetric cell with different electrolyte.

Exchange current densities were calculated by the following equation:

$$i \approx i_0 \frac{F}{RT} \frac{\eta}{2}$$

where i, i_0, η, F, R and T were current density, exchange current density, overpotential, faraday constant, gas constant and absolute temperature, respectively.

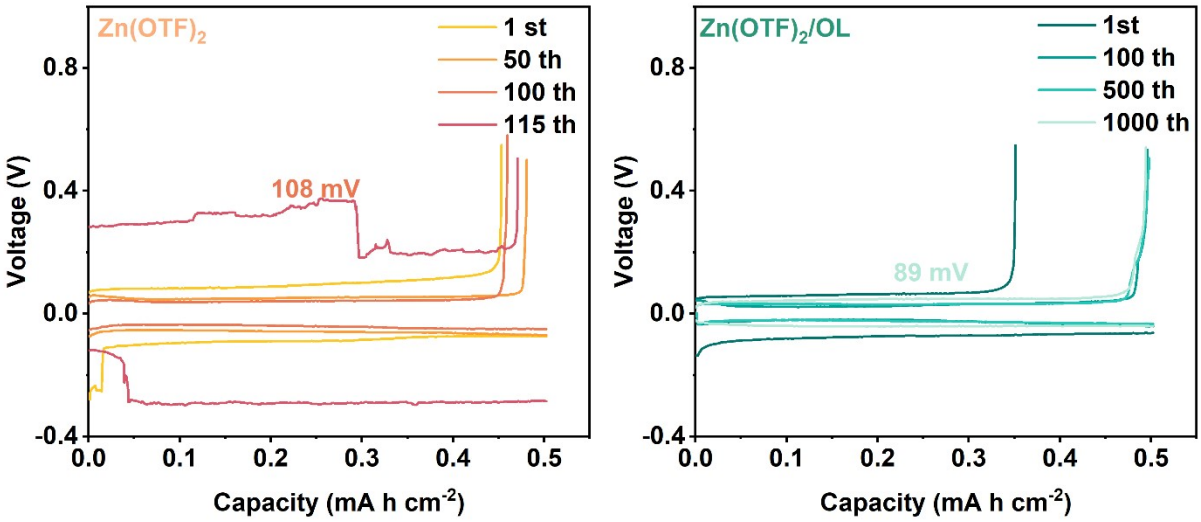

Figure S24. Voltage profiles of the Zn||Cu cells in different electrolytes at different cycles.

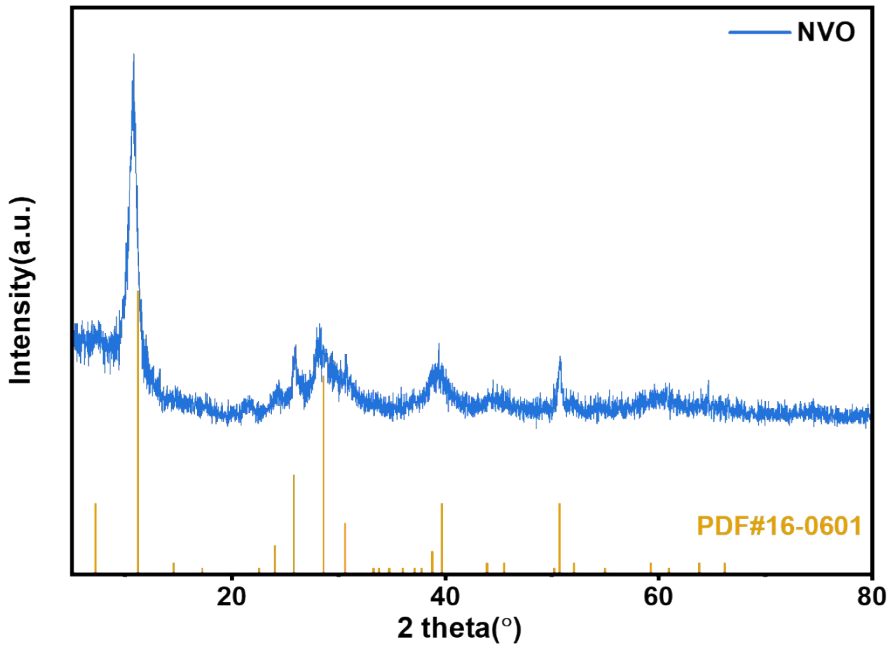

Figure S25. XRD pattern of NVO.

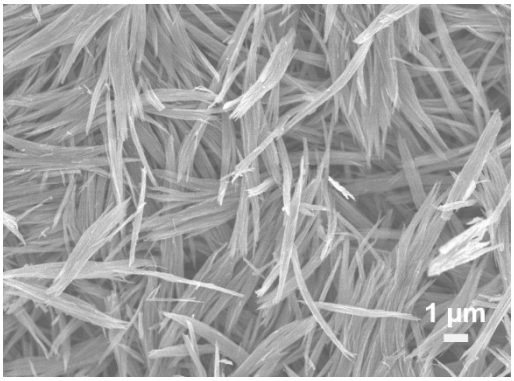

Figure S26. SEM image of NVO.

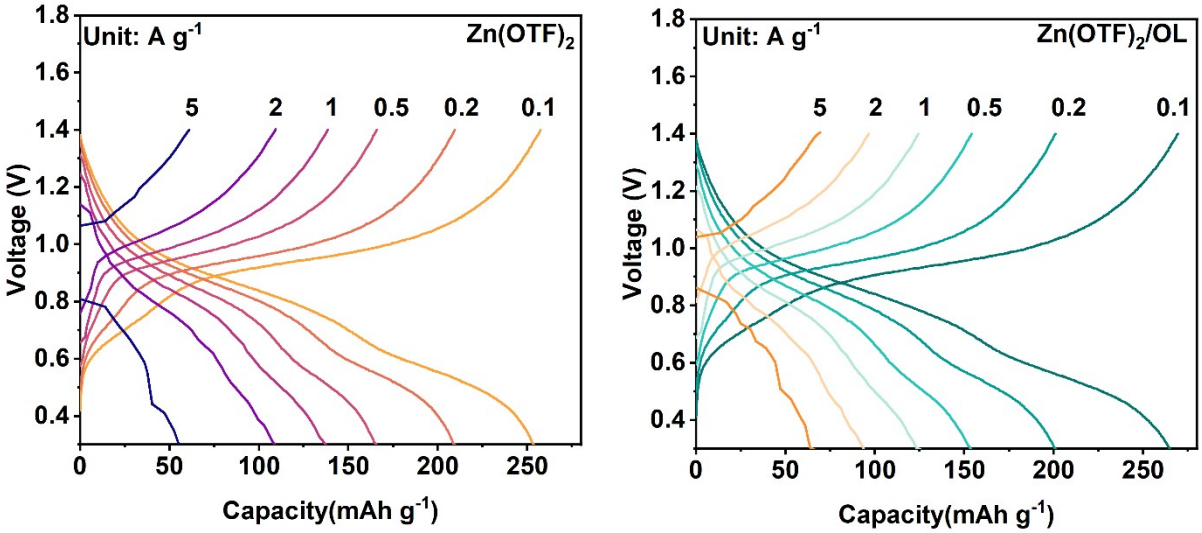

Figure S27. Charge–discharge curves of Zn||NVO with and without OL.

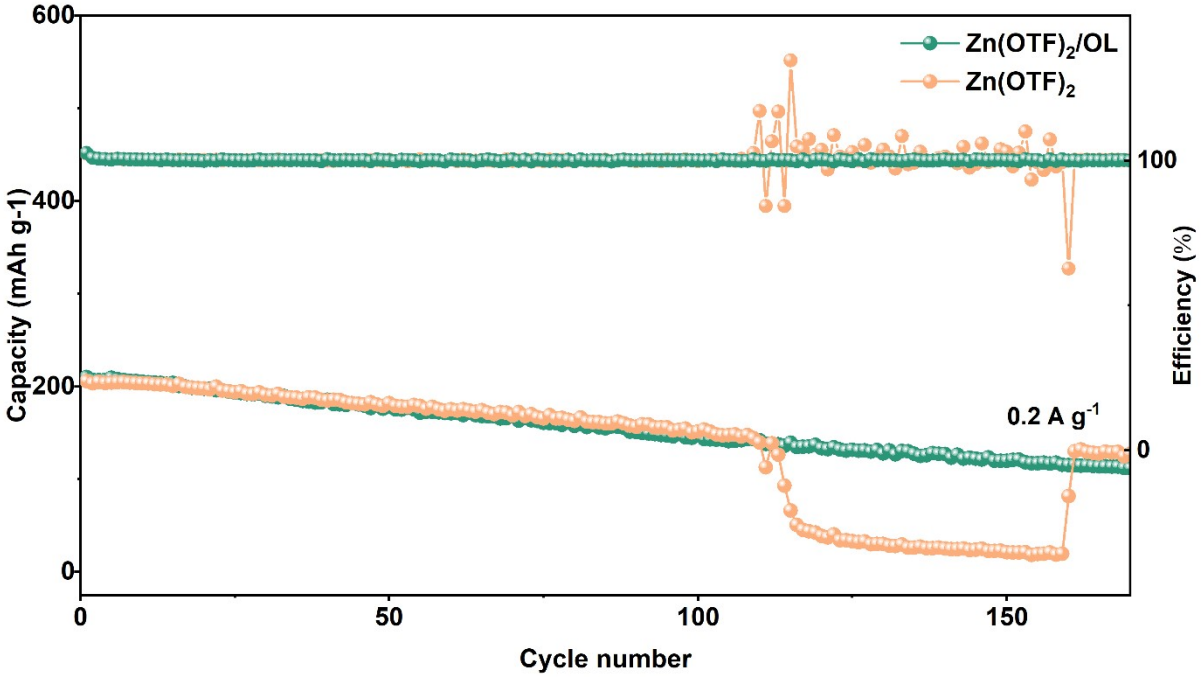

Figure S28. Cycling performance of full cells in different electrolytes at 0.2 A g^{-1}.

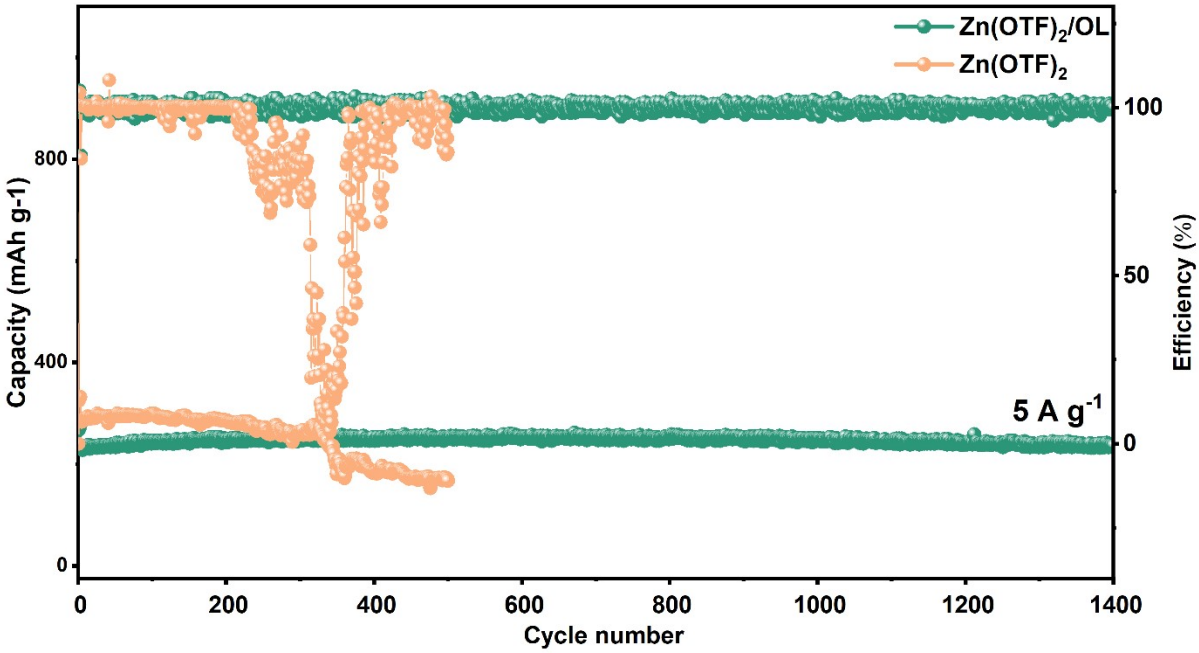

Figure S29. Cycling performance of full cells in different electrolytes at 5 A g^{-1}.

3. Supplementary tables

Table S1: The comparison of capacity and lifespan reported in this work with other previous reports.

Electrolyte	Current density (mA cm^{-2})	Capacity (mA h cm^{-2})	Lifespan(h)	Ref
1M $Zn(OTF)_2$+ 2% Polystyrene sulfonate (PSS)	1	1	3000	5
1M $ZnSO_4$+0.2M potassium Iodide (KI)	5	5	400	6
7.6m $ZnCl_2$+0.05m $SnCl_2$	3	3	500	7
2M $ZnSO_4$+20 vol% dimethyl sulfoxide (DMSO)	1	1	2100	8
	3	3	200	
1M $Zn(OTF)_2$+50% poly (ethylene glycol) dimethyl ether (PEGDME)	1	1	2000	9
0.1M $ZnSO_4$+10% acetonitrile (AN)	1	2	600	10
1M $Zn(OTF)_2$+70% Tetrahydrofurfuryl alcohol (THFA)	1	1	2750	11
2M $ZnSO_4$+0.05mM tetrabutylammonium sulfate (TBA_2SO_4)	2	2	300	12
	5	2	456	
1M $ZnSO_4$+10mM glucose	1	1	2700	13
	5	5	270	
0.5 M $ZnCl_2$ +3-1 0.5M triethylamine hydrochloride	1	0.5	670	14
	3	1.5	560	

(TEHC)				
1M $Zn(OTF)_2$+5 vol% hexamethylphosphoramide (HMPA)	1	1	1500	[15]
2m $Zn(OTF)_2$+7.5% vol Oxolane (OL)	1	1	3200	**This work**
	5	5	520	

Table S2. The number of solution components for the considered OL 0, OL 7.5 and OL 40 systems.

System	Number of solution component			
	Zn^{2+}	$CF_3SO_3^-$	H_2O	OL
OL 0	50	100	1389	0
OL 7.5	50	100	1284	26
OL 40	50	100	833	139

4. Reference:

1. F. Wan, L. Zhang, X. Dai, X. Wang, Z. Niu and J. Chen, Aqueous rechargeable zinc/sodium vanadate batteries with enhanced performance from simultaneous insertion of dual carriers, *Nature communications*, 2018, **9**, 1-11.
2. N. Chang, T. Li, R. Li, S. Wang, Y. Yin, H. Zhang and X. Li, An aqueous hybrid electrolyte for low-temperature zinc-based energy storage devices, *Energy & Environmental Science*, 2020, **13**, 3527-3535.
3. M. D. Segall, J. D. L. Philip, M. J. Probert, C. J. Pickard, P. J. Hasnip, S. J. Clark and M. C. Payne, First-principles simulation: ideas, illustrations and the CASTEP code, *Journal of Physics: Condensed Matter*, 2002, **14**, 2717.
4. J. P. Perdew, K. Burke and M. Ernzerhof, Generalized Gradient Approximation Made Simple, *Physical Review Letters*, 1996, **77**, 3865-3868.
5. Y. Wu, T. Zhang, L. Chen, Z. Zhu, L. Cheng, S. Gu, Z. Li, Z. Tong, H. Li, Y. Li, Z. Lu, W. Zhang and C. S. Lee, Polymer Chain-Guided Ion Transport in Aqueous Electrolytes of Zn-Ion Batteries, *Advanced Energy Materials*, 2023, **13**, 2300719.
6. S. Wang, Y. Zhao, H. Lv, X. Hu, J. He, C. Zhi and H. Li, Low-Concentration Redox-Electrolytes for High-Rate and Long-Life Zinc Metal Batteries, *Small*, **n/a**, 2207664.
7. L. Cao, D. Li, F. A. Soto, V. Ponce, B. Zhang, L. Ma, T. Deng, J. M. Seminario, E. Hu and X. Q. Yang, Highly Reversible Aqueous Zinc Batteries enabled by Zincophilic–Zincophobic Interfacial Layers and Interrupted Hydrogen-Bond Electrolytes, *Angewandte Chemie International Edition*, 2021, **60**, 18845-18851.
8. D. Feng, F. Cao, L. Hou, T. Li, Y. Jiao and P. Wu, Immunizing Aqueous Zn Batteries against Dendrite Formation and Side Reactions at Various Temperatures via Electrolyte Additives, *Small*, 2021, 2103195.
9. Z. Hou, Z. Lu, Q. Chen and B. Zhang, Realizing wide-temperature Zn metal anodes through concurrent interface stability regulation and solvation structure modulation, *Energy Storage Materials*, 2021.
10. Z. Hou, H. Tan, Y. Gao, M. Li, Z. Lu and B. Zhang, Tailoring desolvation kinetics enables stable zinc metal anodes, *Journal of Materials Chemistry A*, 2020, **8**, 19367-19374.
11. Y. Qiu, X. Zheng, R. Zhang, Q. Lin, M. Li, J. Luo, S. Yang, Z. Liu, Q. Wang, Y. Yu and C. Yang, Boosting Zinc-Ion Batteries with Innovative Ternary Electrolyte for Enhanced Interfacial Electrochemistry and Temperature-Resilient Performance, *Advanced Functional Materials*, **n/a**, 2310825.
12. A. Bayaguud, X. Luo, Y. Fu and C. Zhu, Cationic surfactant-type electrolyte additive enables three-dimensional dendrite-free zinc anode for stable zinc-ion batteries, *ACS Energy Letters*, 2020, **5**, 3012-3020.
13. P. Sun, L. Ma, W. Zhou, M. Qiu, Z. Wang, D. Chao and W. Mai, Simultaneous Regulation on Solvation Shell and Electrode Interface for Dendrite-Free Zn Ion Batteries Achieved by a Low-Cost Glucose Additive, *Angewandte Chemie International Edition*, 2021, **60**, 18247-18255.
14. L. Qian, W. Yao, R. Yao, Y. Sui, H. Zhu, F. Wang, J. Zhao, C. Zhi and C. Yang, Cations Coordination-Regulated Reversibility Enhancement for Aqueous Zn-Ion Battery, *Advanced Functional Materials*, 2021, **31**, 2105736.
15. M. Kim, J. Lee, Y. Kim, Y. Park, H. Kim and J. W. Choi, Surface Overpotential as a Key Metric for the Discharge–Charge Reversibility of Aqueous Zinc-Ion Batteries, *Journal of the American Chemical Society*, 2023, **145**, 15776-15787.